

Quantum walk processes in quantum devices

Anandu Kalleri Madhu,¹ Alexey A. Melnikov,^{2,3,*}

Leonid E. Fedichkin,^{3,4} Alexander Alodjants,⁵ and Ray-Kuang Lee^{1,6,7,8}

¹*Department of Physics, National Tsing Hua University, Hsinchu 30013, Taiwan*

²*Terra Quantum AG, 9400 Rorschach, Switzerland*

³*Valiev Institute of Physics and Technology, Russian Academy of Sciences, 117218 Moscow, Russia*

⁴*Moscow Institute of Physics and Technology, 141700 Moscow Region, Russia*

⁵*ITMO University, 197101 St. Petersburg, Russia*

⁶*Institute of Photonics Technologies, National Tsing Hua University, Hsinchu 30013, Taiwan*

⁷*Physics Division, National Center for Theoretical Sciences, Hsinchu 30013, Taiwan*

⁸*Center for Quantum Technology, Hsinchu 30013, Taiwan*

(Dated: December 29, 2020)

The quantum walk process represents a basic subroutine in many quantum algorithms and plays an important role in studying physical phenomena. Quantum particles, photons and electrons, are naturally suited for simulating quantum walks in systems of photonic waveguides and quantum dots. With an increasing improvement in qubits fidelity and qubits number in a single register, there is also potential to substantially improve quantum walks simulations. However, efficient ways to simulate quantum walks in qubit registers still has to be explored. Here different possibilities to efficiently implement quantum walks on IBM Q devices are studied. A mapping from a graph space to quantum register space is provided, and simulations on IBM Q quantum computer are performed. Implemented quantum walks are compared against classically simulated solutions. With this work we examine quantum walks paradigm for IBM Q computer which may exhibit quantum advantage for the algorithms incorporating random walk. Provided solution to quantum walk simulation opens a route to applied quantum algorithms based on quantum walks.

INTRODUCTION

Random walks on graphs naturally appear in different physical processes [1–4] and computational subroutines [5–9]. In order to study these physical processes and implement algorithms, there is a need for efficient ways to simulate random walks [10, 11]. Quantum walks, quantum analogs of (classical) random walks [12–16], similarly naturally appear in physical processes when studied at a quantum level. Quantum interference, which is at the heart of quantum walks [17–22], potentially enables to accelerate transport phenomenon in Fenna-Matthews-Olson (FMO) complexes [23–25] and quantum photonic circuits [26]. Simulating quantum processes is significant for the current state of the art of quantum chemistry [27, 28] and constitutes one of the main applications for quantum computing [29–31]. Moreover, the speed-up problem for quantum walks on the graphs with complex architecture that reproduce transport processes in physical systems represents a sophisticated problem, see, e.g., Refs. [32, 33]. In this regard, simulating quantum walks in existing quantum devices, especially in quantum computers available now, represents an important task for further practical implementations. However, computer simulation of quantum walks is not that straightforward compared to random walks [34–36].

In this work we study practical possibilities to run quantum walk processes in quantum devices. We first consider different implementation scenarios, and then test these implementations by running quantum walks on IBM Q quantum devices with up to 20 physical qubits

and circuit depth of up to 26.

The remainder of the paper is structured as follows. First, an introduction to quantum walks and their simulation is given. Next, quantum walks on hypercube graphs are simulated using two different methods to map graphs on a qubit register. Then a general case of arbitrary graphs is tackled. We provide a methodology to map a space of unitaries to a space of graphs. Finally, both theoretical analysis and practical implementation on IBM Q devices are performed. As a result, we provide procedures for simulating quantum walks on gate-based quantum computers.

Simulating quantum walks on graphs

Single particle continuous-time quantum walks (CTQW) on graphs are studied in this paper. A quantum particle can be located in one of the d positions on a graph with d vertices, or in a superposition of these positions. A quantum state of this particle can be thought of as a state of a d -level system $|\psi_d(t)\rangle = \sum_{i=0}^{d-1} \alpha_i(t) |i\rangle$, with $|\alpha_i(t)|^2$ being the detection probability in vertex i at time t . Evolution of this quantum state is governed by the Hamiltonian with nearest-neighbour hopping terms

$$\mathcal{H}_A = \hbar\Omega \sum_{i,j=0}^{d-1} A_{ij} |i\rangle \langle j| = \hbar\Omega A, \quad (1)$$

where A is an adjacency matrix of a graph on which quantum walk is performed, A_{ij} are the elements of this

matrix, and Ω is the hopping frequency.

The unitary quantum state evolution is hence a solution to the Schrödinger equation, which is given by

$$|\psi_d(t)\rangle = e^{-i\Omega t A} |\psi_d(0)\rangle. \quad (2)$$

Note that A is not necessarily symmetric – the weights A_{ij} are complex parameters and can, in general, lead to a chiral quantum walk on a weighted graph [37, 38].

Exponentiation of the $\Omega t A$ matrix is computationally hard for large d . In the case of using a quantum computer, however, it is known that some unitary matrices can be efficiently implemented in time logarithmic in d . However, as the form of a Hermitian matrix A is arbitrary, we cannot efficiently implement any quantum walk on a quantum computer. In the general case, the matrix A is described by $(d^2 - d)/2$ independent complex-valued variables, which means in the worst case, one would need to apply $O(d^2)$ operations making exponential speedup impossible. In this paper we explore the set of matrices A , for which efficient implementation is possible, and demonstrate this implementation on the IBM Q quantum device.

QUANTUM WALKS ON HYPERCUBES

In this section we discuss the implementation of a CTQW of a particle on n -dimensional hypercube graphs. Hypercube graphs represent a starting point towards studying complex graphs. In order to simulate quantum walks on hypercubes, one needs to establish a mapping. Firstly, an encoding of the particle’s position in the space of qubits needs to be defined. Secondly, a sequence of quantum gates must be specified, which corresponds to a unitary defined by an adjacency matrix. Here we consider two possibilities of mappings, although there could be more, which correspond to an exponential reduction of the number of qubits compared to the graph vertices. The first possibility is based on using separable qubits, whereas the second possibility requires entangled qubits. In both cases the state $|\psi_d(t)\rangle$ is simulated on a classical simulator and IBM Q quantum devices.

Simulation with separable qubits

The first mapping is demonstrated in Fig. 1(a). Instead of describing a quantum particle’s position as a state of a single d -level quantum system, we can think of the position as a state of an $n = \log d$ qubits system. These two different ways of encoding a quantum walker state are shown in Fig. 1(a) for cube graphs. Both cube graphs in Fig. 1(a) have the same adjacency matrix A^{hc} . The two graphs’ difference is only in the vertex labeling: decimal (left cube, from 0 to 7) and binary (right

cube, from 000 to 111) encoding choices. The binary encoding choice replaces a d -level quantum system, qudit, with multiple 2-level systems, qubits.

In addition to the quantum walkers state mapping, we also specify the mapping for unitary operations defined by the graph edges. The binary labeling shown in Fig. 1(a) on the right helps us seeing that two vertices are connected by a bit-flip operation. Moreover, each i -th bit-flip corresponds to a walk on the i -th axis. Therefore, a walk on a hypercube is a sequence of independent bit-flip operations. In other words, CTQW on an arbitrary n -dimensional hypercube can be decomposed into CTQW on n independent line graphs. The same can be observed by decomposing the A^{hc} matrix:

$$A^{\text{hc}} = \sum_{i=0}^{n-1} I_2^{\otimes i} \otimes A_i^{\text{line}} \otimes I_2^{\otimes n-1-i}. \quad (3)$$

Moreover, as a direct consequence of the above identity, the unitary matrix that is a function of A is equal to

$$U(A^{\text{hc}}) = e^{-i\Omega t A^{\text{hc}}} = \left(e^{-i\Omega t A^{\text{line}}} \right)^{\otimes n}, \quad (4)$$

where $A^{\text{line}} = |0\rangle\langle 1| + |1\rangle\langle 0|$ represents an adjacency matrix of a two-vertex line graph.

We next implement the CTQW on n -dimensional hypercubes in qubit registers of IBM Q. Because of the unitary operations simplified form, obtained in Eq. (4), we implement n identical CTQW on a line. Each quantum walk on the line is simulated by a single-qubit unitary that evolves the qubit state $|\psi_2^{(i)}\rangle$ shown in Fig. 1(a). For the simulation, we use the U_3 gate in Qiskit to evolve the CTQW during the time $t = \theta/2\Omega$:

$$U_3(\theta, \phi, \lambda) = \begin{bmatrix} \cos \frac{\theta}{2} & -e^{i\lambda} \sin \frac{\theta}{2} \\ e^{i\phi} \sin \frac{\theta}{2} & e^{i(\lambda+\phi)} \cos \frac{\theta}{2} \end{bmatrix}. \quad (5)$$

A combined CTQW circuit, which is composed out of the U_3 gates, is depicted in Fig. 1(b). The initial position of the simulated particle is defined by the initial quantum state $|\psi_{2^n}(0)\rangle = |\psi_2^{(1)}(0)\rangle \otimes \dots \otimes |\psi_2^{(n)}(0)\rangle$. Because of the symmetry of hypercube graphs, without the loss of generality, the initial vertex will always be “00...0” and $|\psi_{2^n}(0)\rangle = |00\dots 0\rangle$. Simulating the evolution of $|\psi_{2^n}(t)\rangle$ with the specified initial condition, we observe detection probabilities $p_k = |\langle k|\psi_{2^n}(t)\rangle|^2$ by repeating the circuit execution on the IBM Q quantum device.

As a result of the simulations, we obtained the particle’s probability to be in different vertices of the hypercubes in different time steps. The results for graphs with $n = 3$ and $n = 20$ are given in Fig. 1(c) and Fig. 1(d), respectively. The results demonstrate that starting from the “00...0” initial node, the quantum particle moves along the graph reaching the furthest node “11...1” with almost unit probability at time $t = \pi/2\Omega$. The same

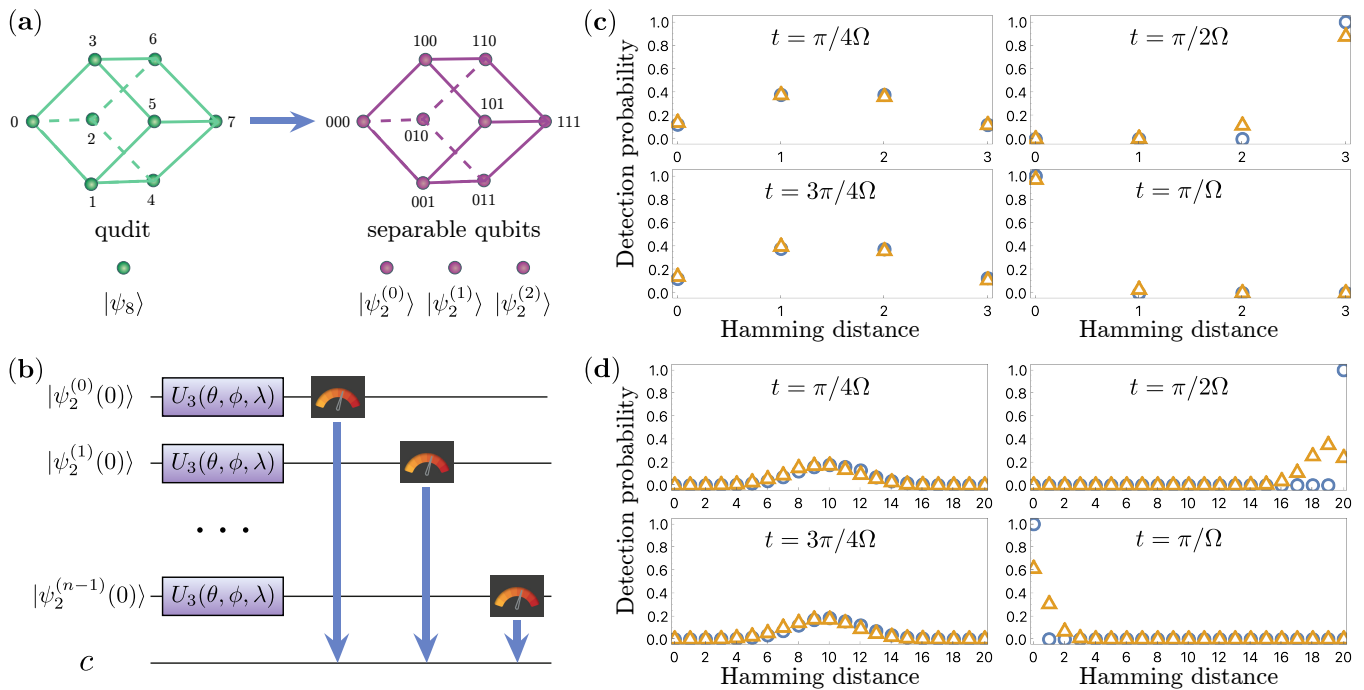


FIG. 1. (a) Two different ways to encode a state of a walking particle on a hypercube graph: one qudit (left), and n separable qubits (right). (b) Quantum circuit for a CTQW implemented on n separable qubits. (c)-(d) Quantum and classical simulation of CTQW on a 3-dimensional hypercube (c) and a 20-dimensional hypercube (d). Each plot shows a probability distribution of particle position on a graph at different times, corresponding to quantum circuit parameters $\phi = -\pi/2, \lambda = \pi/2$ and $\theta = 2\Omega t = \pi/2, \pi, 3\pi/2, 2\pi$. The blue circles and orange triangles correspond to execution on the quantum IBM Q device and the classical simulator, respectively. Hamming distance indicates the distance at which particle propagated starting from the initial state labeled as “00...0”.

holds for both $n = 3$ and $n = 20$. Indeed, for any dimension n , the time for a perfect particle transfer is constant $t = \pi/2\Omega$. This is expected since we evolved the walk through separable qubits independently. In the results shown in Fig. 1(c)-(d), classical simulated results are shown as blue circles and quantum simulated results are shown as orange triangles. We observe that for times $t = \pi/4\Omega$ and $t = 3\pi/4\Omega$ the quantum simulated probability distribution matches the classical simulated probability distribution with an error in probability below 0.05 for all data points. In cases of $t = \pi/2\Omega$ and $t = \pi/\Omega$, however, the errors in quantum simulation go up to 0.15 for $n = 3$, and up to 0.8 for $n = 20$. In addition, the errors are counter-intuitively lower for $t = \pi/\Omega$ compared to $t = \pi/2\Omega$, which is explained by the underlying quantum system symmetry.

Simulation with entangled qubits

A different mapping can be used to simulate a CTQW on a hypercube. In this mapping, one exploits the fact that there is an equal probability of detecting a particle in vertices with the same Hamming distance. By taking all the symmetries into account, one obtains a weighted

line graph. The mapping procedure is shown in Fig. 2 for $n = 3$ (a) and $n = 4$ (b). The Hamiltonian that governs the quantum walk in the mapped space can be defined for an arbitrary n :

$$H^{\text{hc} \rightarrow \text{line}} = \sum_{i=0}^n \beta_{i,i+1} (X_i X_{i+1} + Y_i Y_{i+1}), \quad (6)$$

where $\beta_{i,i+1} = \sqrt{i(n+1-i)}$ are the couplings between qubits, $X = |0\rangle\langle 1| + |1\rangle\langle 0|$ and $Y = -i|0\rangle\langle 1| + i|1\rangle\langle 0|$ are the Pauli matrices. Implementing a quantum walk in this mapping has an advantage of the exponential reduction of the number of qubits, as there is only $(n+1)$ qubits needed for n -dimensional hypercube CTQW implementation. This is similar to the mapping with separable qubits considered before, which required n qubits.

For the simulation of CTQW on a hypercube with this mapping, we have to implement the above Hamiltonian in Eq. (6) on the IBM quantum computer. Since the terms of the Hamiltonian do not commute, we use the Trotter decomposition to simulate the Hamiltonian. The corresponding quantum circuit obtained for the CTQW simulation is given in Fig. 2(c). The circuit consists of the CNOT, U_1 , U_2 , and U_3 gates applied to four qubits.

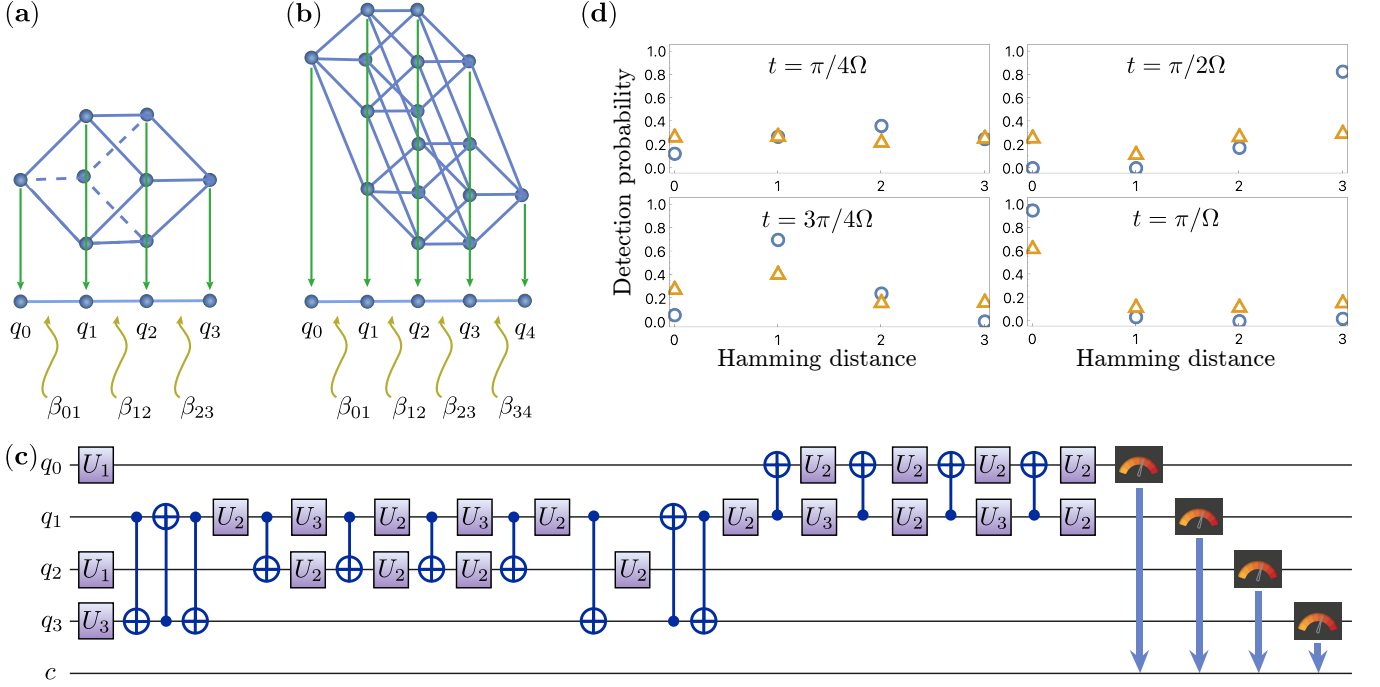


FIG. 2. (a)-(b) Mapping an n -dimensional hypercube graph to a line graph. Examples for $n = 3$ (a) and $n = 4$ (b) are shown. Weights β are defined in Eq. (6). (c) Quantum circuit for a CTQW implemented on four entangled qubits. (d) Quantum and classical simulation results for mapping a 3-dimensional cube to a weighted line with 4 vertices. Each plot shows a probability distribution of particles position on a graph at different times: $t = \pi/4\Omega$, $\pi/2\Omega$, $3\pi/4\Omega$, and π/Ω . The blue circles and orange triangles correspond to execution on the simulator and the IBM Q quantum register, respectively. Hamming distance indicates the distance at which particle propagated starting from the initial state corresponding to an excited state of the q_0 qubit.

U_2 gate is defined as

$$U_2 \equiv U_3(\pi/2, \phi, \lambda) = \begin{bmatrix} 1 & -e^{i\lambda} \\ e^{i\phi} & e^{i(\lambda+\phi)} \end{bmatrix}, \quad (7)$$

whereas U_1 gate is defined

$$U_1 \equiv U_3(0, 0, \lambda) = \begin{bmatrix} 1 & 0 \\ 0 & e^{i\lambda} \end{bmatrix}. \quad (8)$$

In this mapping, the nodes of the line are encoded using one-hot encoding. In this encoding, the states are represented by bit strings, which consist of “1” at nodes where the particle can be found and zeros elsewhere. Therefore, the total Hilbert space of the CTQW gets reduced to these states. The described encoding helps in error-correcting all the other states those are not valid in the one-hot encoding, which we obtain while implementing the CTQW on IBM Q devices.

For $n = 3$ hypercube, which is shown in Fig. 2(a), we can compare this evolution of the CTQW mapped to a line with the CTQW implemented on individual qubits as shown in Fig. 1(c). We observe that the walk’s evolution on each time step is similar for both implementations if we correct the experimental errors occurring

during the implementation. The quantum and classical simulation results are shown in Fig. 2(d). Compared to the simulation results in Fig. 1(c), the probabilities mismatch has two origins: errors because of the Trotterization procedure, and error because of the larger depth of the experimental quantum circuit. In both Fig. 1 and Fig. 2, the transport between opposite hypercube vertices should be noticed. In the case of the implementation shown in Fig. 2, it also corresponds to transport in quantum spin networks [39].

QUANTUM WALKS ON ARBITRARY GRAPHS

Not all unitary operations are efficiently implementable on a quantum computer, hence not all graphs A with d vertices can be implemented with $O(\log d)$ qubits in time $O(\text{poly}(\log d))$. Nonetheless, as we demonstrated in the previous section, for the hypercube graphs it is possible. By studying CTQW on hypercubes, and providing different implementations of the same process, we conclude that some implementations are more feasible than others. To see what other graphs have a feasible and efficient implementation on a quantum device, we propose the following.

To find out which graphs can be efficiently imple-

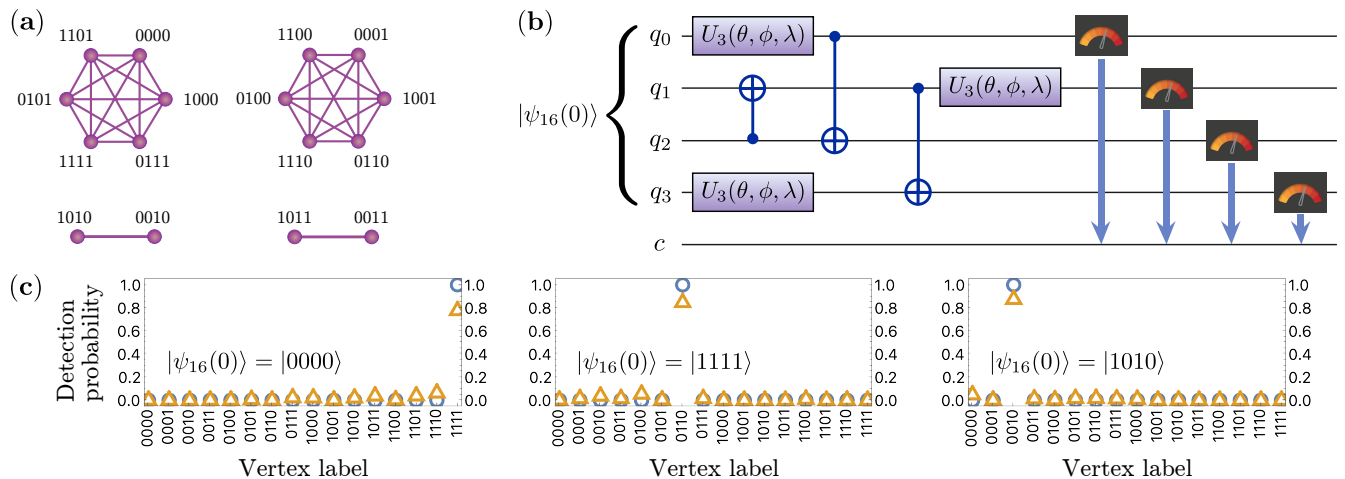


FIG. 3. (a) A weighted graph generated from a 4-qubit quantum circuit with U_3 and CNOT gates on which we evolved a CTQW starting from the node “0000” and ending up in “1111” with probability one. Weights are not shown. (b) A 4-qubit quantum circuit consisting of U_3 and CNOT gates with a circuit depth of 5. (c) Quantum and classical simulation results for a quantum walk on the graph (a). Each plot shows a probability distribution of particles position on a graph for different initial conditions: $|\psi_{16}(0)\rangle = |0000\rangle$, $|1111\rangle$, and $|1010\rangle$. The blue circles and orange triangles correspond to execution on the simulator and the IBM Q quantum register, respectively. Vertex labels correspond to vertices in (a).

mented on a quantum computer, we explore different quantum circuits that are efficiently implementable on the IBM Q quantum computer. Each of these quantum circuits represents some specific unitary operation U , which has a corresponding adjacency matrix $A(U)$. Because of the form of evolution $U = e^{-i\Omega t A}$ in Eq. (2), $A(U) = i \log(U)/\Omega t$. The logarithm of a unitary matrix is not uniquely defined, however [40]. First, adding a term $2\pi k I$, $k \in \mathcal{Z}$ with I being the identity matrix does not introduce a change in the matrix A . Second, adding a global phase $c \in \mathcal{C}$ to a unitary $U' = cU$ does not change the particles quantum walk dynamics. The freedom in phase leads to a possibility to add a term φI , $\varphi \in \mathcal{R}$ to any adjacency matrix without affecting the quantum walk simulation. Third, one adds a complete graph with a factor $2\pi k A_{\text{complete}}/n\Omega t$, $k \in \mathcal{Z}$, without introducing a change in U . This is a consequence of A_{complete}/n being an idempotent matrix with n – number of qubits. Finally, combining all three possibilities to modify A together, we obtain

$$A = \frac{i}{\Omega t} \log(U) + \varphi I + \frac{2\pi k}{n\Omega t} A_{\text{complete}}, \quad (9)$$

with free parameters $k \in \mathcal{Z}$, and $\varphi \in \mathcal{R}$. In addition to the derived Eq. (9), multiplying A by an arbitrary factor $b \in \mathcal{R}$ leads to an effective rescaling of the transition frequency $\Omega' = \Omega/b$, which broadens the set of available A even more.

The derived Eq. (9) helps us obtain a variety of adjacency matrices of potential interest given the unitary transformation. Our implementation of the unitary transformations, in turn, is adjusted to the quantum device’s connectivity. From the quantum device’s connec-

tivity limitations, it is possible to simulate which $U(A)$ are easily implementable with k -depth quantum circuits. For this, we automated sampling of random circuits that implement a perfect transport from the state “0...00” to the state “1...11” with a circuit depth up to 5. We obtained these circuits to find feasible U , and from it feasible graphs $A(U)$. In the case of 4 qubits, we obtained a graph shown in Fig. 3(a), by randomly implementing U_3 and CNOT gates. The corresponding quantum circuit is given in Fig. 3(b). Given that the initial state is “0000”, the circuit’s transformation is equivalent to unitary in Eq. (4). However, for the general initial particle’s position, i.e., general $|\psi_{16}(0)\rangle$, the transformation is different from the hypercubes cases. This difference can be observed from the disconnected graph shown in Fig. 3(a) compared to a fully connected graph of a 4-dimensional cube in Fig. 2(b). Quantum and classical simulation results in Fig. 3(c) demonstrate the chiral nature of the graph. Indeed, starting from $|\psi_{16}(0)\rangle = |0000\rangle$, particle ends in $|1111\rangle$, however starting from $|\psi_{16}(0)\rangle = |1111\rangle$ brings the particle to the “0110” vertex. The simulations performed for the initial state $|\psi_{16}(0)\rangle = |1010\rangle$ shows that particle is bounded to the subspace of the “1010” and “0010” vertices. Note that fidelities of all the quantum simulations in Fig. 3 are above 0.75.

CONCLUSION

Implementation of continuous-time quantum walks is studied and performed in this paper. Quantum walks are implemented utilizing classical and quantum simulation, where quantum simulations are performed on currently available quantum computers of IBM Q. All quantum walks implementations are performed with qubits, which number scale logarithmically with the graph size.

The presented results consist of two parts. First, quantum walks on the family of hypercube graphs were implemented via two different schemes showing qubit circuits' versatility. The used schemes were compared in their implementations on IBM Q. The scheme involving only separable qubits is advantageous in terms of the number of gates and overall fidelity, whereas the scheme involving entangled qubits is better suited for other platforms. Second, a scheme for quantum simulation of continuous-time quantum walks on arbitrary graphs was presented. We found graphs on which quantum walks are efficiently simulated by defining adjacency matrices as unitary operations functions. We were then able to find feasible graphs from unitary operations, and implement quantum walks on IBM Q. With our work, we hence established an analogy between quantum circuits and graphs.

This work paves the way towards practical, efficient implementation of quantum walks on graphs. We believe that future work could be centered around the automated classification of graphs for understanding which graphs are efficiently implementable with quantum circuits [32, 33].

ACKNOWLEDGMENTS

This work was financially supported by the Grant of RFBR, No 19-52-52012 MHT_a. R.K.L. acknowledges funding by the Ministry of Science and Technology of Taiwan (No. 109-2112-M-007-019-MY3, 109-2627-M-008-001, 108-2923-M-007-001-MY3). The investigation was supported by Program No. 0066-2019-0005 of the Ministry of Science and Higher Education of Russia for Valiev Institute of Physics and Technology of RAS.

* Corresponding author, e-mail: alexey@melnikov.info

- [1] M. Kac, Random walk and the theory of Brownian motion, *Am. Math. Mon.* **54**, 369 (1947).
- [2] F. Bartumeus, M. G. E. da Luz, G. M. Viswanathan, and J. Catalan, Animal search strategies: A quantitative random-walk analysis, *Ecology* **86**, 3078 (2005).
- [3] D. Brockmann, L. Hufnagel, and T. Geisel, The scaling laws of human travel, *Nature* **439**, 462 (2006).
- [4] E. A. Codling, M. J. Plank, and S. Benhamou, Random walk models in biology, *J. Royal Soc. Interface* **5**, 813 (2008).
- [5] R. Motwani and P. Raghavan, *Randomized algorithms* (Cambridge University Press, New York, USA, 1995) Chap. 6.
- [6] F. Wang and D. P. Landau, Efficient, multiple-range random walk algorithm to calculate the density of states, *Phys. Rev. Lett.* **86**, 2050 (2001).
- [7] T. Sottinen, Fractional Brownian motion, random walks and binary market models, *Financ. Stoch.* **5**, 343 (2001).
- [8] K. K. Sabelfeld and N. A. Simonov, *Random walks on boundary for solving PDEs* (Walter de Gruyter, 2013).
- [9] C. Gkantsidis, M. Mihail, and A. Saberi, Random walks in peer-to-peer networks: Algorithms and evaluation, *Perform. Eval.* **63**, 241 (2006).
- [10] D. T. Gillespie, Monte Carlo simulation of random walks with residence time dependent transition probability rates, *J. Comp. Phys.* **28**, 395 (1978).
- [11] M. B. Cohen, J. Kelner, J. Peebles, R. Peng, A. Sidford, and A. Vladu, Faster algorithms for computing the stationary distribution, simulating random walks, and more, in *57th Annual Symposium on Foundations of Comp. Sci.* (2016) pp. 583–592.
- [12] Y. Aharonov, L. Davidovich, and N. Zagury, Quantum random walks, *Phys. Rev. A* **48**, 1687 (1993).
- [13] J. Kempe, Quantum random walks: An introductory overview, *Contemp. Phys.* **44**, 307 (2003).
- [14] N. Konno, Quantum walks, in *Quantum potential theory* (Springer, 2008) pp. 309–452.
- [15] S. E. Venegas-Andraca, Quantum walks: a comprehensive review, *Quantum Inf. Process.* **11**, 1015 (2012).
- [16] L. Fedichkin and F. Meshchaninov, Analysis and applications of quantum walks, *Journal of Mathematical Sciences* **252**, 104 (2020).
- [17] H. Krovi and T. A. Brun, Hitting time for quantum walks on the hypercube, *Phys. Rev. A* **73**, 032341 (2006).
- [18] D. Solenov and L. Fedichkin, Continuous-time quantum walks on a cycle graph, *Phys. Rev. A* **73**, 012313 (2006).
- [19] L. Fedichkin, D. Solenov, and C. Tamon, Mixing and decoherence in continuous-time quantum walks on cycles, *Quantum Inf. Comput.* **6**, 263 (2006).
- [20] A. A. Melnikov and L. E. Fedichkin, Quantum walks of interacting fermions on a cycle graph, *Sci. Rep.* **6**, 34226 (2016).
- [21] Q.-P. Su, Y. Zhang, L. Yu, J.-Q. Zhou, J.-S. Jin, X.-Q. Xu, S.-J. Xiong, Q. Xu, Z. Sun, K. Chen, et al., Experimental demonstration of quantum walks with initial superposition states, *npj Quantum Information* **5**, 1 (2019).
- [22] W.-X. Cui, Y. Xing, L. Qi, X. Han, S. Liu, S. Zhang, and H.-F. Wang, Quantum walks in periodically kicked circuit qed lattice, *Opt. Express* **28**, 13532 (2020).
- [23] G. S. Engel, T. R. Calhoun, E. L. Read, T.-K. Ahn, T. Mančal, Y.-C. Cheng, R. E. Blankenship, and G. R. Fleming, Evidence for wavelike energy transfer through quantum coherence in photosynthetic systems, *Nature* **446**, 782 (2007).
- [24] M. Mohseni, P. Rebentrost, S. Lloyd, and A. Aspuru-Guzik, Environment-assisted quantum walks in photosynthetic energy transfer, *J. Chem. Phys.* **129**, 174106 (2008).

- [25] E. Harel and G. S. Engel, Quantum coherence spectroscopy reveals complex dynamics in bacterial light-harvesting complex 2 (LH2), *PNAS* **109**, 706 (2012).
- [26] F. Flamini, N. Spagnolo, and F. Sciarrino, Photonic quantum information processing: a review, *Rep. Prog. Phys.* **82**, 016001 (2018).
- [27] R. Babbush, P. J. Love, and A. Aspuru-Guzik, Adiabatic quantum simulation of quantum chemistry, *Sci. Rep.* **4**, 6603 (2014).
- [28] P. J. J. O’Malley, R. Babbush, I. D. Kivlichan, J. Romero, J. R. McClean, R. Barends, J. Kelly, P. Roushan, A. Tranter, N. Ding, B. Campbell, Y. Chen, Z. Chen, B. Chiaro, A. Dunsworth, A. G. Fowler, E. Jeffrey, E. Lucero, A. Megrant, J. Y. Mutus, M. Neeley, C. Neill, C. Quintana, D. Sank, A. Vainsencher, J. Wenner, T. C. White, P. V. Coveney, P. J. Love, H. Neven, A. Aspuru-Guzik, and J. M. Martinis, Scalable quantum simulation of molecular energies, *Phys. Rev. X* **6**, 031007 (2016).
- [29] I. M. Georgescu, S. Ashhab, and F. Nori, Quantum simulation, *Rev. Mod. Phys.* **86**, 153 (2014).
- [30] A. M. Childs, D. Maslov, Y. Nam, N. J. Ross, and Y. Su, Toward the first quantum simulation with quantum speedup, *Proceedings of the National Academy of Sciences* **115**, 9456 (2018).
- [31] J. Bermejo-Vega, D. Hangleiter, M. Schwarz, R. Raussendorf, and J. Eisert, Architectures for quantum simulation showing a quantum speedup, *Phys. Rev. X* **8**, 021010 (2018).
- [32] A. A. Melnikov, L. E. Fedichkin, and A. Alodjants, Predicting quantum advantage by quantum walk with convolutional neural networks, *New J. Phys.* **21**, 125002 (2019).
- [33] A. A. Melnikov, L. E. Fedichkin, R.-K. Lee, and A. Alodjants, Machine learning transfer efficiencies for noisy quantum walks, *Advanced Quantum Technologies* **3**, 1900115 (2020).
- [34] J. A. Izaac and J. B. Wang, pyCTQW: A continuous-time quantum walk simulator on distributed memory computers, *Comput. Phys. Commun.* **186**, 81 (2015).
- [35] P. Falloon, J. Rodriguez, and J. Wang, QSWalk: A mathematics package for quantum stochastic walks on arbitrary graphs, *Comput. Phys. Commun.* **217**, 162 (2017).
- [36] S. Apers, A. Sarlette, and F. Ticozzi, Simulation of quantum walks and fast mixing with classical processes, *Phys. Rev. A* **98**, 032115 (2018).
- [37] Z. Zimboras, M. Faccin, Z. Kadar, J. D. Whitfield, B. P. Lanyon, and J. Biamonte, Quantum transport enhancement by time-reversal symmetry breaking, *Sci. Rep.* **3**, 2361 (2013).
- [38] D. Lu, J. D. Biamonte, J. Li, H. Li, T. H. Johnson, V. Bergholm, M. Faccin, Z. Zimborás, R. Laflamme, J. Baugh, and S. Lloyd, Chiral quantum walks, *Phys. Rev. A* **93**, 042302 (2016).
- [39] M. Christandl, N. Datta, A. Ekert, and A. J. Landahl, Perfect state transfer in quantum spin networks, *Phys. Rev. Lett.* **92**, 187902 (2004).
- [40] T. A. Loring, Computing a logarithm of a unitary matrix with general spectrum, *Numer. Linear Algebra Appl.* **21**, 744 (2014).

SUPPLEMENTAL INFORMATION

In this section we provide a table of parameters for the quantum circuit used in Fig. 2(c).

All 4-qubit circuits were executed on the “ibmq-bogota” IBM quantum processor, and all 20-qubit circuits were executed on the “ibmq-paris” IBM quantum processor.

Parameters	U_3 Gates																			
	1	2	3	4	5	6	7	8	9	10	11	12	13	14	15	16	17	18	19	20
θ	1.57	0	1.57	0	3.14	1.57	3.14	1.57	1.57	1.57	1.57	1.57	3.14	1.57	3.14	1.57	1.57	1.57	1.57	1.57
ϕ	3.14	0	0	0	0.96	-1.14	0.96	-1.14	-1.57	-3.14	-1.57	-3.14	0.96	-1.14	0.96	-1.14	-1.57	4.71	-1.57	-4.71
λ	3.14	4.71	0	4.71	2.54	-4.71	2.54	-4.71	-3.14	4.71	-3.14	4.71	2.54	-4.71	2.54	-4.71	-1.57	4.71	-1.57	-1.57

TABLE I. The gate parameters used in the circuit in Fig. 2(c) are given in the order from top to bottom, left to right. For simplicity, parameters are shown in the U_3 gate notation, even though gates of U_1 and U_2 were used in the circuit.